IEEE Access
Multidisciplinary | Rapid Review | Open Access Journal

Received January 1, 2020, accepted January 20, 2020, date of publication January 27, 2020, date of current version February 4, 2020.

Digital Object Identifier 10.1109/ACCESS.2020.2969488

Broadband and Low-Profile Penta-Polarization Reconfigurable Metamaterial Antenna

PENG LIU, WEN JIANG, (Member, IEEE), SHANGYI SUN, YAN XI, AND SHUXI GONG, (Member, IEEE)

National Key Laboratory of Antennas and Microwave Technology, Xidian University, Xi'an 710071, China

Corresponding author: Wen Jiang (jw13@vip.qq.com)

This work was supported in part by the National Basic Research Program of China-973 Program under Grant 2015CB857100, and in part by the National Key Research and Development Program of China under Grant 2017YFF0205200.

ABSTRACT In this paper, a penta-polarization reconfigurable antenna with mushroom-type metamaterial loading is proposed, which can operate in x-direction linear polarization (x-LP), y-LP, 45°-LP, left-hand circular polarization (LHCP) and right-hand circular polarization (RHCP). In order to realize polarization reconfigurability, a dual-port dual LP mushroom antenna excited by crossed H-shape slot is designed by characteristic mode analysis (CMA). Through shifting the states of PIN diodes on the reconfigurable feeding network, the amplitude and phase distributions of two ports of the dual LP antenna can be dynamically controlled and the five polarization modes can be achieved. A prototype with a profile of $0.06\lambda_0$ at 5.2 GHz (λ_0 is the operated wavelength in free space) is simulated and measured. The measurement results exhibit a wide impedance bandwidth over 33.2% for LPs and over 38.7% for CPs. In addition, the measured axial ratio bandwidths are 28.0% for LHCP and 30.3% for RHCP, and the maximum measured boresight gains of all modes are higher than 8.2 dBi. The simulated and measured results verify that the proposed antenna can achieve a balance between low-profile and broadband on the basis of penta-polarization reconfigurability. The proposed antenna can be applied to polarization diversity and C band satellite communication.

INDEX TERMS Broadband antenna, characteristic mode analysis (CMA), low-profile, metamaterial (MTM), PIN diode, polarization reconfigurable antenna.

I. INTRODUCTION

With the evolution of modern wireless communication, the polarization diversity of antenna has been extensively studied. In order to enhance the performance of the communication system such as channel capacity, frequency reuse, multipath fading, and polarization mismatch, a polarization diversity technique using polarization reconfigurable antennas has been widely presented in the open literature. In available works, conventional patch antennas generally possess electrically small profile but their bandwidth is narrow, whereas wideband antennas generally possess higher thicknesses. It is a big challenge to achieve a balance between low-profile and broadband for a multi-polarization reconfigurable antenna.

By properly adjusting the current distributions on the radiator, the polarization of antennas can be dynamically controlled. There are two main techniques to implement polarization reconfigurable antennas. One technique is shifting the structure of the antenna radiator. By introducing PIN diodes on the patch, reconfigurable omnidirectional antennas are obtained [1], [2]. A wideband polarization reconfigurable magneto-electric dipole can realize three polarization modes with a profile of $0.21\lambda_0$ (λ_0 is the wavelength in free space at the center operated frequency) [3]. The polarization of the antenna can be switched among linear polarization (LP), left-hand circular polarization (LHCP) and right-hand circular polarization (RHCP) by mechanically changing the relative positions of the polarization conversion metasurface and the slot antenna [4], [5]. The fractional bandwidth of the antenna in [4] is 11.4% with a profile of $0.02\lambda_0$. Due to the loading of the metasurface and the metallic reflector, the antenna has a fractional bandwidth of 33.3% and can achieve the maximum gain of 16.5 dBi with a profile of $0.74\lambda_0$ in [5]. In [6], the linearly polarized waves of a planar slot antenna can be rotated to either left-hand or right-hand circular polarized waves via electronically adjusting the polarizer, which realizes a working bandwidth of 1.6% and a low profile of $0.09\lambda_0$.

The other technique to generate polarization reconfigurability is employing reconfigurable feeding structure. With the

The associate editor coordinating the review of this manuscript and approving it for publication was Raghvendra Kumar Kumar Chaudhary.

T-shape feed loaded by diodes, a patch antenna exhibits reconfigurability between the LHCP and RHCP, whose overlapped operation bandwidth is only 2.27% [7]. This antenna has a peak gain of 7.26 dBi and a height of $0.15\lambda_0$. Three multi-polarization reconfigurable antennas with reflective grounds are designed by utilizing the crossed dipole antenna [8]–[10]. All of them have wideband impedance bandwidth, but their height is over $0.14\lambda_0$. Through placing PIN diodes across the cross-slot etched on the ground, a crossed slot coupled dual-polarization reconfigurable low-profile antenna array without complex feeding network is proposed, and its working bandwidth is 9.3% [11]. With the similar feeding structure in [11], the overlapped bandwidth of the polarization reconfigurable dielectric resonator antenna in [12] has been increased to 20.7%. The partially reflective surface (PRS) contributes to improving the gain and bandwidth of antennas, which is adopted to design antennas with switchable feeding network [13], [14]. However, the PRS is placed above the antennas, thus the height of two antennas is above $0.5\lambda_0$. In [15], a quad-polarization reconfigurable low-profile antenna with metasurface loading has been designed by using a square patch as the radiation source, whose working bandwidth is less than 20%. Overall, in the design of a multi-polarization reconfigurable antenna, it is quite difficult to achieve low-profile and wideband characteristics simultaneously.

Metamaterial (MTM) is an artificially constructed periodic or non-periodic array structure composed of subwavelength cells, moreover the two-dimensional metamaterial is also called metasurface [16]. According to performance, it can be divided into polarization conversion metasurface, PRS, composite right/left-handed (CRLH) structure, and electromagnetic band gap, etc. Using MTM as the radiation patch or reflector, the antennas in [17]–[23] exhibit excellent performance in bandwidth, profile, and gain. Mushroom type is a typical CRLH structure, which is usually used to the radiation patch of antenna. With the TM_{10} and TM_{20} modes, the mushroom antennas in [17] and [20] have realized the broadband working and boresight radiation.

For overcoming the difficulty mentioned above, a crossed H-shaped slot coupled penta-polarization reconfigurable antenna with mushroom-type metamaterial loading is proposed in this paper. By appropriately altering the on/off status of the diodes soldered on the feeding network, the polarization of the proposed antenna can be switched among x-LP, y-LP, 45°-LP, LHCP and RHCP. Because the MTM directly acts as a radiator, the proposed antenna can realize broadband working bandwidth and low-profile simultaneously.

II. DESIGN OF THE DUAL LP ANTENNA

The x and y electric field components of the plane electromagnetic wave can be expressed as

$$\begin{aligned} \overrightarrow{E}_x &= \widehat{x}E_{xm}e^{j\varphi_x} \\ \overrightarrow{E}_y &= \widehat{y}E_{ym}e^{j\varphi_y}. \end{aligned} \tag{1}$$

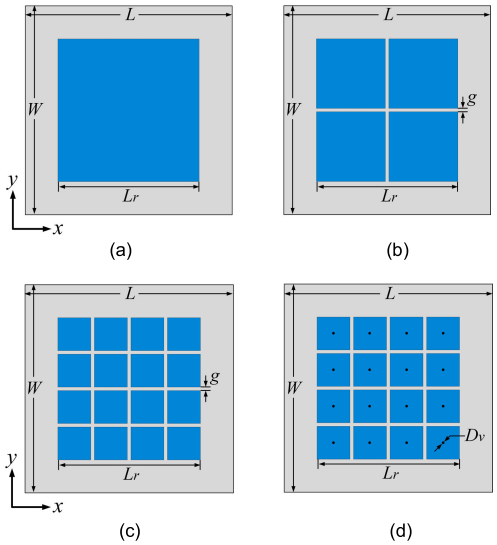

FIGURE 1. Four radiation structures. (a) Case I. (b) Case II. (c) Case III. (d) Case IV.

When the x-component and y-component have the different amplitude and phase, the polarization of the plane electromagnetic wave can be controlled as follow.

- When $E_{ym} = 0$, x-LP is obtained.
- When $E_{xm} = 0$, y-LP is obtained.
- When $E_{xm} = E_{ym}$, $\varphi_{xm} = \varphi_{ym}$, 45°-LP is obtained.
- When $E_{xm} = E_{ym}$, φ_{xm} - $\varphi_{ym} = 90°$, RHCP is obtained.
- When $E_{xm} = E_{ym}$, φ_{xm} - $\varphi_{ym} = -90°$, LHCP is obtained.

In order to achieve the above functions, the dual LP antenna is a good choice. The different polarization modes can be generated by controlling the amplitude and phase distributions of two ports of a dual LP antenna. Therefore, for a low-profile, broadband multi-polarization reconfigurable antenna, it is necessary to design a high-performance dual LP antenna first.

A. THE SELECTION OF RADIATION STRCYURE WITH CHARACTERISTIC MODE ANALYSIS

The transmission-line model is a common method to analyze MTM structure in the antenna design [17], [20], but it is unable to provide the radiation behavior of the finite periodic structure. Characteristic mode analysis (CMA) provides insight into the radiation property of arbitrary shape without the extra source. Therefore, in order to reveal the working mechanism of the antenna, four radiation structures printed on the F4B substrate with complete ground are analyzed by the theory of characteristic mode in CST Studio Suite. The four radiation structures with the same overall size are shown in Fig. 1. The 3 mm thick substrate has the permittivity of $\varepsilon_r = 3.5$. The modal significances (MSs) of four structures are depicted in Fig. 2.

In CMA [24], there is a generalized eigenvalue equation

$$\boldsymbol{X}\boldsymbol{J}_n = \lambda_n \boldsymbol{R}\boldsymbol{J}_n \tag{2}$$

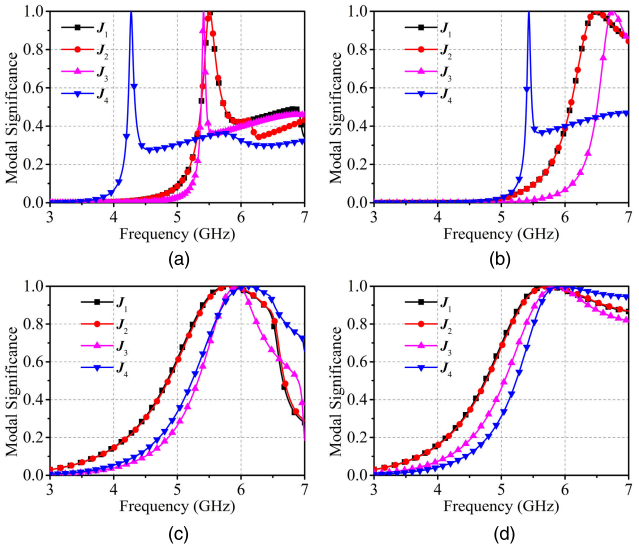

FIGURE 2. MSs of four structures. (a) Case I. (b) Case II. (c) Case III. (d) Case IV.

here eigenvalues λ_n and eigenvectors $\boldsymbol{J}_\mathrm{n}$ are real, and the index n represents the order of each mode. The Hermitian matrices $\boldsymbol{R}$ and $\boldsymbol{X}$ are the real and imaginary parts of impedance matrix

$$\boldsymbol{Z} = \boldsymbol{R} + j\boldsymbol{X} \tag{3}$$

Characteristic modes contain a set of complete orthogonal modes. The induced currents and the induced far-fields can be written as

$$\boldsymbol{J} = \sum_n a_n \boldsymbol{J}_n \tag{4}$$

$$\boldsymbol{E} = \sum_n a_n \boldsymbol{E}_n \tag{5}$$

where a_n is the complex model weighting coefficient (MWC) of mode $\boldsymbol{J}_\mathrm{n}$ and represents the contribution of each mode. The MWC a_n can be further given as

$$a_n = \frac{\langle \boldsymbol{E}_i \cdot \boldsymbol{J}_n \rangle}{1 + j\lambda_n} \tag{6}$$

$\boldsymbol{E}_\mathrm{i}$ is called the impressed electric field and the inner product $\langle \boldsymbol{E}_i \cdot \boldsymbol{J}_n \rangle$ is a guideline of the feeding position. MS is defined as

$$\mathrm{MS} = \left| \frac{1}{1 + j\lambda_n} \right| \tag{7}$$

it characterizes the coupling ability of mode $\boldsymbol{J}_\mathrm{n}$ under the external source. The mode may be radiated efficiently when MS ≥ 0.7, and it is deemed as the resonant frequency when MS $= 1$. Therefore, the operated band can be estimated from Fig. 2. Fig. 3 shows the modal currents and modal radiation patterns at the corresponding resonant frequencies of four structures.

In view of obtaining a dual LP antenna, a pair of orthogonal linear polarization modes with broadside radiation is wanted,

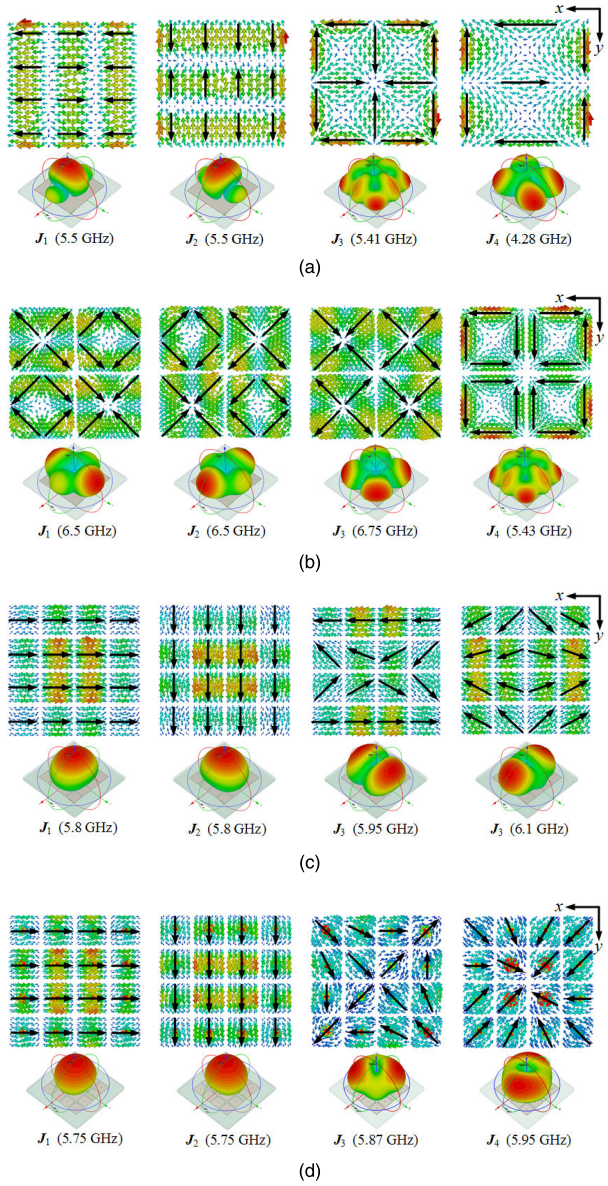

FIGURE 3. Modal currents and corresponding modal radiation patterns of four structures. (a) Case I. (b) Case II. (c) Case III. (d) Case IV.

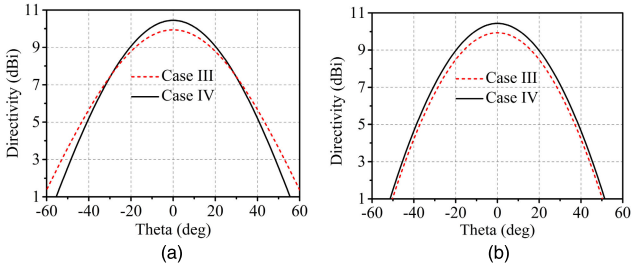

FIGURE 4. Modal radiation patterns of Case III and Case IV at 5.75 GHz. (a) *xoz*-plane. (b) *yoz*-plane.

namely, an x-LP mode and a y-LP mode. It is observed that the modes $\boldsymbol{J}_1$ and $\boldsymbol{J}_2$ of Case I have the same MS curves and they are two desired orthogonal linear polarization modes

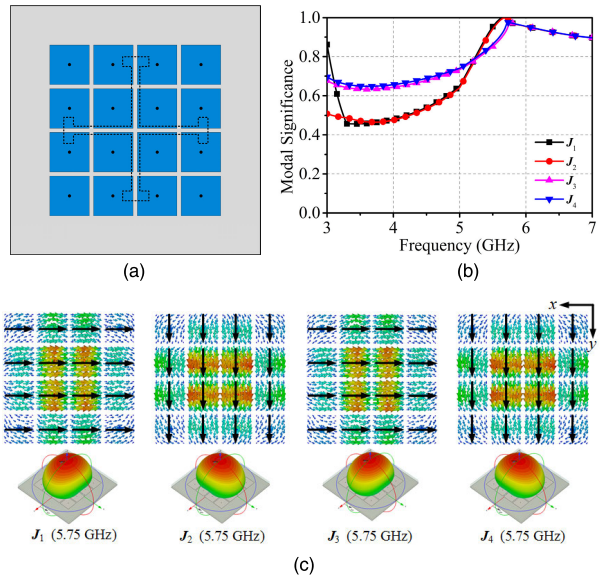

FIGURE 5. (a) Configuration, (b) MSs, (c) modal currents and the corresponding modal radiation patterns of Case IV with slot.

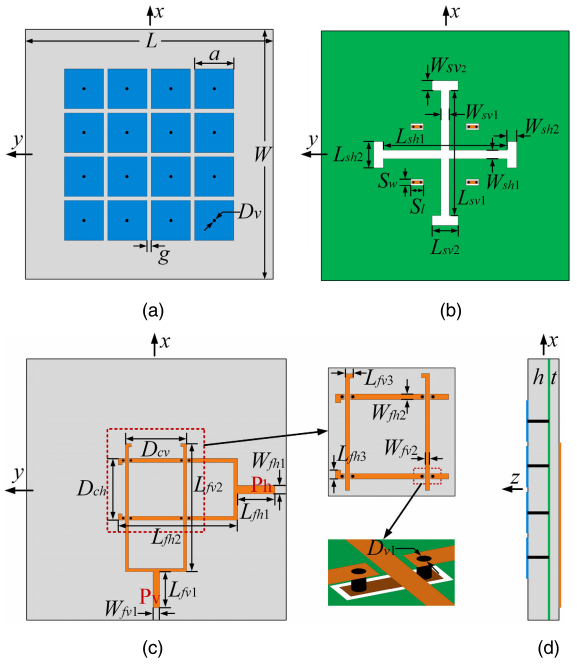

FIGURE 6. Configuration of the dual LP antenna. (a) Top layer. (b) Ground layer. (c) Bottom layer. (d) Side view.

with broadside radiation. As for $\boldsymbol{J}_3$ and $\boldsymbol{J}_4$, they are unwanted modes. However, the resonant bands of modes $\boldsymbol{J}_1$ and $\boldsymbol{J}_2$ are narrow and the patterns of them have side lobes owing to the anti-phase currents. Case II has etched grid-slot based on Case I. In Fig. 3(b), the radiation patterns of four modes appear nulls in boresight directions due to the strong anti-phase currents, although the resonant bands of $\boldsymbol{J}_1$ and $\boldsymbol{J}_2$ modes are improved in Fig. 2(b). Therefore, all modes of Case II are unwanted. Furthermore, the Case III and Case IV with periodic subwavelength cells are designed, and they are MTM structure. Here, Case IV increases metal vias based on the Case III. From Fig. 2 and Fig. 3, the mode $\boldsymbol{J}_1$ and mode $\boldsymbol{J}_2$ of two structures have the same MS curves, modal currents and radiation patterns, which are a pair of desired orthogonal linear polarization modes with broadside radiation. The resonant bands of them have been increased, too. The mode $\boldsymbol{J}_3$ and $\boldsymbol{J}_4$ of two structures show radiation nulls because of the out-of-phase currents, which are undesired modes.

For comparison, Fig. 4 shows the modal radiation patterns of $\boldsymbol{J}_1$ mode of two structures, which come from two main cut planes at 5.75 GHz. Because both of two structures are rotated symmetric, the performance of $\boldsymbol{J}_2$ mode are analogous to $\boldsymbol{J}_1$ mode. It is seen that the directivity of Case IV is 0.5 dBi greater than Case III. In consequence, the gain produced by Case IV will be higher than the Case III under the same excited structure, which is validated by [17] and [18]. Consequently, the Case IV is adopted in this paper.

B. CHARACTERISTIC MODE ANALYSIS OF RADIATION STRCYURE WITH SLOT

For exciting the $\boldsymbol{J}_1$ and $\boldsymbol{J}_2$ modes of the Case IV, a ground with crossed H-shaped slot is designed as depicted in Fig. 5(a). The MSs, modal currents and modal radiation patterns of Case IV with the slotted ground at 5.75 GHz are depicted in Fig. 5(b) and Fig. 5(c), respectively. Here the four modes are two pair of desired orthogonal LP modes. Combined with Fig. 2(d), it is obvious that the MSs of $\boldsymbol{J}_1$ and $\boldsymbol{J}_2$ modes in Fig. 5(b) are significantly enhanced in the range of 3-5 GHz and are roughly unchanged from 5 GHz to 7 GHz. And the mode $\boldsymbol{J}_3$ and $\boldsymbol{J}_4$ are two new modes in consideration of the resonant frequency in Fig. 2(d). As a result, the potential operation bandwidth is significantly broadened after introducing the crossed H-shaped slot.

C. THE DUAL LP ANTENNA WITH METAMATERIAL LOADING

With the Case IV as the radiation patch, the configuration of the proposed dual LP antenna is depicted in Fig. 6. Three metallic layers are printed on two F4B substrates. And both substrates have the same permittivity of $\varepsilon_r = 3.5$ and loss tangent of $\tan\delta = 0.002$. The total thickness of two substrates is 3.5 mm, and corresponding relatively height is $0.06\lambda_0$ at 5.2 GHz. Fig. 6(a) shows the top layer of the antenna, which is the mushroom-type MTM structure. Fig. 6(b) shows the crossed H-shaped slot coupled structure. According to the CMA, the x-LP and y-LP modes of the MTM are two desired modes. In order to excite the x-LP and y-LP modes, two crossed Y-shaped feeding lines are designed as shown in Fig. 6(c). For reducing the number of the dielectric substrate, two feeding strips are designed on the same layer. The horizontal polarization Y-shaped feeding line is bridged connected as shown in the inset, which avoids the overlapping of two feeding lines. The implementation method is to etch the rectangular slots on the ground layer and then connect the

TABLE 1. Parameters of the dual LP antenna.

Label	Value (mm)	Label	Value (mm)	Label	Value (mm)
L	60	W_{sh1}	1.8	L_{fh3}	1.45
W	60	W_{sh2}	1.7	W_{fh1}	1.9
h	3	L_{sv1}	30.6	W_{fh2}	0.9
t	0.508	L_{sv2}	5	L_{fv1}	8.15
a	9.5	W_{sv1}	1.8	L_{fv2}	29.2
g	0.9	W_{sv2}	1.7	L_{fv3}	1.35
D_v	0.4	Sl	3.1	W_{fv1}	1.5
D_{v1}	0.4	S_w	1.1	W_{fv2}	0.7
L_{sh1}	30.6	L_{fh1}	8.55	D_{ch}	13.9
L_{sh2}	5	L_{fh2}	26.9	D_{cv}	13.7

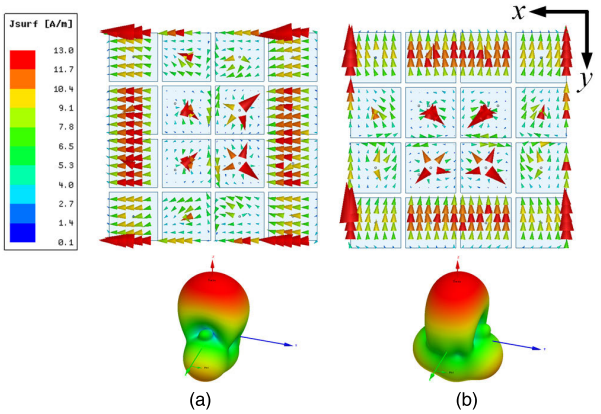

FIGURE 7. Simulated surface current distributions and the corresponding modal radiation patterns at 5.75 GHz of the dual LP antenna. (a) *x*-LP. (b) *y*-LP.

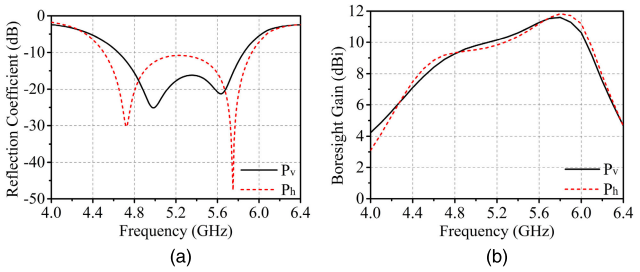

FIGURE 8. Simulated reflection coefficients and boresight gains of the dual LP antenna. (a) Reflection coefficients. (b) Boresight gains.

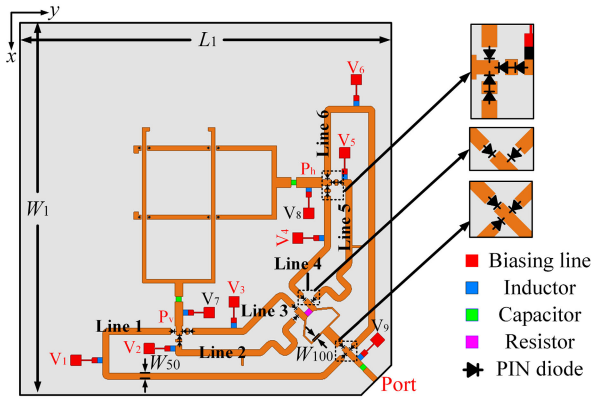

FIGURE 9. Geometrical configuration of the reconfigurable feeding network.

cut-off horizontal Y-shaped strip through short metallic vias and short strips. The detailed three-dimensional parameters of the dual LP antenna are listed in Table 1.

The dual LP antenna is simulated by the high frequency simulation software ANSYS HFSS. For verifying the performance of the feeding structure, Fig. 7 shows the simulated surface current distributions and the corresponding modal radiation patterns at 5.75 GHz of two LP states. It is can be found that two LP modes are excited effectively and other modes are suppressed. The reflection coefficients and the boresight gains of the dual LP antenna are simulated as shown in Fig. 8. When vertical port (P_v) and horizontal port (P_h) are excited separately, the 10-dB fractional bandwidths of the antenna are 23.1% (4.64-5.85 GHz) and 27.2% (4.51-5.93 GHz). Within the operating band, the antenna has two roughly equal radiation gains vary from 7.8 to 11.6 dBi in two polarized states, which is conducive to designing CP and 45°-LP antenna.

III. DESIGN OF THE RECONFIGURABLE FEEDING NETWORK AND POLARIZATION RECONFIGURABLE ANTENNA

A. DESIGN OF RECONFIGURABLE FEEDING NETWORK

For the sake of the polarization reconfigurability, the reconfigurable feeding network is designed based on the dual LP antenna as shown in Fig. 9, which is symmetric about the diagonal. The silicon PIN diode MA4FCP300 is introduced to shift the polarization by adjusting the states of the PIN diode. As observed in Fig. 10, the diode is equivalent to a parasitic inductance of 0.6 nH in series with a low forward resistance of 2.6 Ω in the on state, and equivalent to a same parasitic inductance in series with a parallel circuit composed of a low reverse bias capacitance of 0.04 pF and a 20K Ω resistor in the off state [25], [26]. For getting the same voltage drop across each diode, some diodes are connected in series as shown in the inset of Fig. 9. The nine 470 nH inductors used between bias lines and microstrip lines act as RF chokes, and three 360 pF capacitors play an important role in AC/DC isolation. The lines with the width of W_{50} and W_{100} correspond to a characteristic impedance of 50 Ω and 100 Ω, respectively. The electrical lengths of Line 2 and Line 5 are 90 degrees longer than Line 3 and Line 4, so that the circular polarization reconfigurability can be realized. The branches on the Line 2 and Line 5 are used to improve axial ratio. The biasing lines V_7, V_8 and V_9 are connected to the negative terminal, and other bias lines are connected to the controlling switches. When the bias lines V_1 and V_6 are set to positive voltage separately, the *x*-LP or *y*-LP will be activated because Line 1 or Line 6 is excited. When the V_2 and V_4 have acquired positive voltage, the Line 2 and Line 4 will be excited, thus the LHCP will be radiated. Analogously, the RHCP will be radiated when the V_3 and V_5 are applied to a positive voltage, and the 45°-LP will be generated when the V_2 and V_5 are applied to positive voltage. All switches

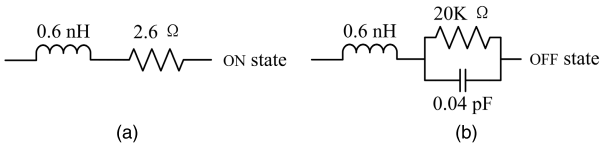

FIGURE 10. Equivalent circuit of the PIN diode in on and off state.

TABLE 2. Switches states on biasing lines and corresponding polarizations.

V_1	V_2	V_3	V_4	V_5	V_6	Polarization
ON	OFF	OFF	OFF	OFF	OFF	x-LP
OFF	OFF	OFF	OFF	OFF	ON	y-LP
OFF	ON	OFF	OFF	ON	OFF	45°-LP
OFF	ON	OFF	ON	OFF	OFF	LHCP
OFF	OFF	ON	OFF	ON	OFF	RHCP

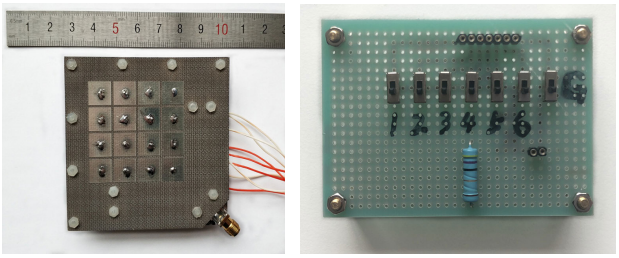

FIGURE 11. Photograph of the fabricated prototype. (a) Antenna. (b) Controlling switches.

states applied to the bias lines and the corresponding polarized states are summarized in Table 2. With the proposed reconfigurable feeding network, the antenna can realize the penta-polarization reconfigurability.

B. SIMULATION AND MEASUREMENT RESULTS

To validate the design above, a prototype of the proposed polarization reconfigurable antenna has been fabricated and measured. Fig. 11(a) shows the photograph of the proposed antenna prototype, whose states of polarization are controlled by six single-pole single-throw (SPST) switches as shown in Fig. 11(b). A 50 Ω current-limiting resistor is used to protect diodes in the bias circuit.

The reflection coefficients are measured by Rohde & Schwarz ZNB 40. The gains, axial ratios and radiation patterns are measured in the anechoic chamber.

In radiation pattern measurement, a high-purity LP rectangular horn antenna is used to measure the amplitude (H_A, V_P) and phase (H_P, V_P) of an antenna under test (AUT). The measurement results only obtain two LP components of the AUT, hence the following elaborates on the formulas of the CP radiation patterns.

The LHCP and RHCP waves can be expressed by two orthogonal horizontal and vertical LP waves [27].

$$E_{LHCP} = \frac{1}{\sqrt{2}}\{[H_A\cos(H_P) + V_A\sin(V_P)] + j[H_A\sin(H_P) - V_A\cos(V_P)]\} \quad (8)$$

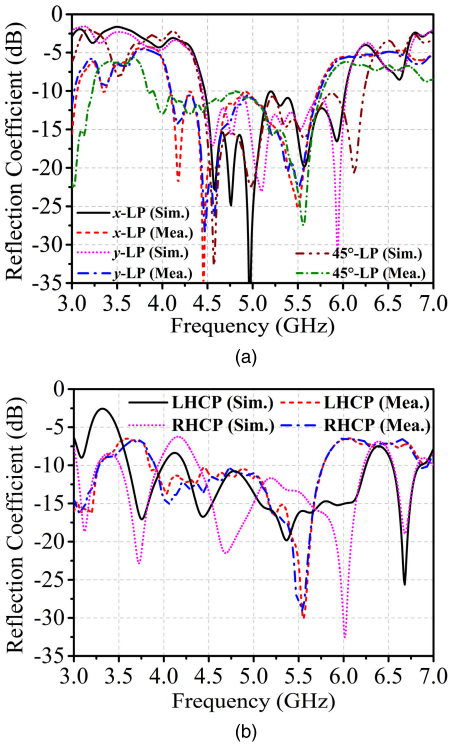

FIGURE 12. Simulated and measured reflection coefficients of the proposed antenna. (a) Three LP modes. (b) Two CP modes.

$$E_{RHCP} = \frac{1}{\sqrt{2}}\{[H_A\cos(H_P) - V_A\sin(V_P)] + j[H_A\sin(H_P) + V_A\cos(V_P)]\} \quad (9)$$

E_{LHCP} and E_{RHCP} are the LHCP and RHCP components. When $|E_{\mathrm{LHCP}}| > |E_{\mathrm{RHCP}}|$, the AUT shows LHCP, otherwise the AUT shows RHCP. The power pattern of each CP can be expressed as

$$P_{LHCP}(dB) = 10\log_{10}\left(\frac{E_{LHCP}^2}{377}\right) \quad (10)$$

$$P_{RHCP}(dB) = 10\log_{10}\left(\frac{E_{RHCP}^2}{377}\right) \quad (11)$$

where 377 Ω is the free-space wave impedance. Furtherly, the axial ratio AR can be obtained by

$$AR = 20\log\left|\frac{|E_{LHCP}| + |E_{RHCP}|}{|E_{LHCP}| - |E_{RHCP}|}\right| \quad (12)$$

The measurement of the gain is realized by substitution method. The method needs to obtain the peak power max $|P_{\mathrm{AUT}}|$ of the AUT, then measure the peak power max $|P_{\mathrm{std}}|$ of the standard gain G_{std} antenna with the same polarization and at the same position as the AUT. The absolute gain G_{AUT} of the AUT is expressed as

$$G_{AUT} = G_{std} + [\max|P_{AUT}| - \max|P_{std}|] \quad (13)$$

With the equations (8) to (13), the measured gains, axial ratios and radiation patterns can be accurately calculated.

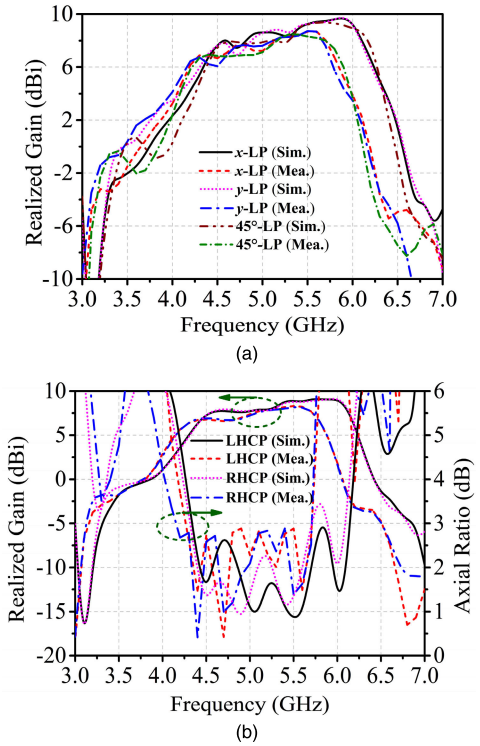

FIGURE 13. Simulated and measured boresight gains and axial ratios of the proposed antenna. (a) Three LP modes. (b) Two CP modes.

TABLE 3. Simulated and measured results at different modes.

Polarization		*x*-LP	*y*-LP	45°-LP	LHCP	RHCP
Impedance BW (GHz)	Sim.	4.47-6.02 (29.6%)	4.45-6.03 (30.2%)	4.43-6.23 (33.8%)	3.61-6.25 (53.5%)	3.52-6.22 (55.4%)
	Mea.	4.09-5.72 (33.2%)	4.09-5.74 (33.6%)	3.84-5.77 (40.2%)	3.84-5.77 (40.2%)	3.9-5.77 (38.7%)
Axial ratio BW (GHz)	Sim.				4.34-6.10 (33.7%)	4.36-5.70 (26.6%)
	Mea.				4.30-5.70 (28.0%)	4.20-5.70 (30.3%)
Maximum gain (dBi)	Sim.	9.74	9.80	9.36	9.11	9.20
	Mea.	8.69	8.73	8.49	8.30	8.20

The simulated and measured reflection coefficients, axial ratios and boresight gains shown in Fig. 12 and Fig. 13 are summarized in Table 3. It is can be found that the measured 10-dB relative impedance bandwidths are higher than 33.2% for three LP states and higher than 38.7% for two CP states. The frequency offset of measured results comes from the deviation of the dielectric constant of the F4B, but the trend of the curves is reasonably consistent with the simulation results. Fig. 13 gives the boresight gains and axial ratios of the proposed antenna. The simulated gains of the proposed antenna have a great reduction compared to dual LP antenna, which resulting from the diode loss. The measured gains are lower than the simulated gains in most operating frequencies for all modes. The degradation is mainly derived from soldering tolerance, imprecise equivalent simulation of PIN diodes, and cable loss. The measured fractional axial ratio bandwidths are 28.0% for LHCP mode and 30.3% for RHCP mode.

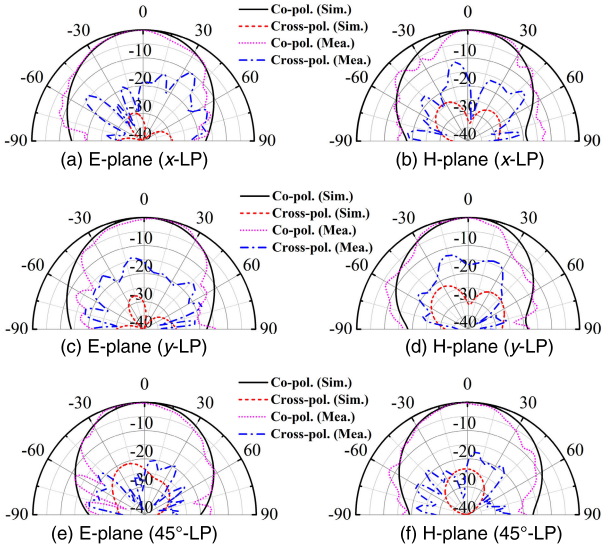

FIGURE 14. Simulated and measured E-plane and H-plane normalized radiation patterns of the proposed antenna at 4.8 GHz. (a) E-plane of *x*-LP. (b) H-plane of *x*-LP. (c) E-plane of *y*-LP. (d) H-plane of *y*-LP. (e) E-plane of 45°-LP. (f) H-plane of 45°-LP.

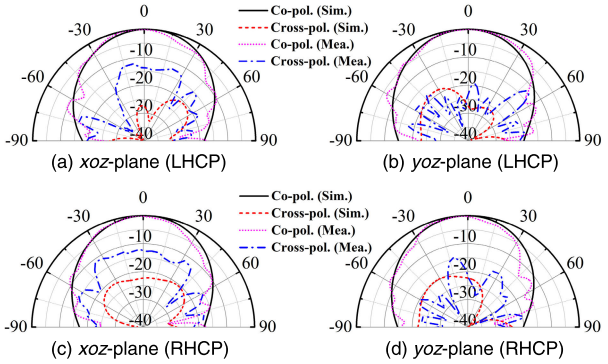

FIGURE 15. Simulated and measured *xoz*-plane and *yoz*-plane normalized radiation patterns of the proposed antenna at 4.8 GHz. (a) *xoz*-plane of LHCP. (b) *yoz*-plane of LHCP. (c) *xoz*-plane of RHCP. (d) *yoz*-plane of RHCP.

TABLE 4. Performance comparison between the proposed antenna and previous works.

Reference	No. of Polarization	Center Frequency (GHz)	Overlapped Bandwidth (%)	Peak Gain (dBi)	Profile (λ_0)	Total Size (λ_0*λ_0)
[3]	3	2.1	33.9	9.0	0.21	0.79×1.05
[4]	3	3.5	11.4	8.4	0.02	0.91×0.91
[5]	3	9.6	33.3	16.5	0.74	2.56×2.56
[6]	2	2.55	1.6	9.6	0.09	1.02×1.02
[7]	2	2.64	2.3	7.3	0.15	0.62×0.62
[8]	5	2.7	37.1	8.9	0.3	0.86×0.86
[9]	4	1.9	35	7.1	0.24	Not give
[10]	4	3.15	53.9	10.9	0.14	0.76×0.76
[11]	2	2.36	9.3	13.5	0.04	3.31×1.26
[12]	3	5.75	20.7	7.3	0.1	1.0×1.0
[13]	3	5	13.1	11.2	0.6	1.83×1.83
[14]	3	2.46	21	15.1	0.5	1.4×1.4
[15]	4	5.6	20	9.39	0.07	1.3×1.3
This work	**5**	**5.2**	**28**	**8.2**	**0.06**	**1.21×1.21**

In Fig. 12, the measured results have shifted toward the low frequency by about 0.4 GHz compared with the simulation results. Therefore, the simulated and measured normalized

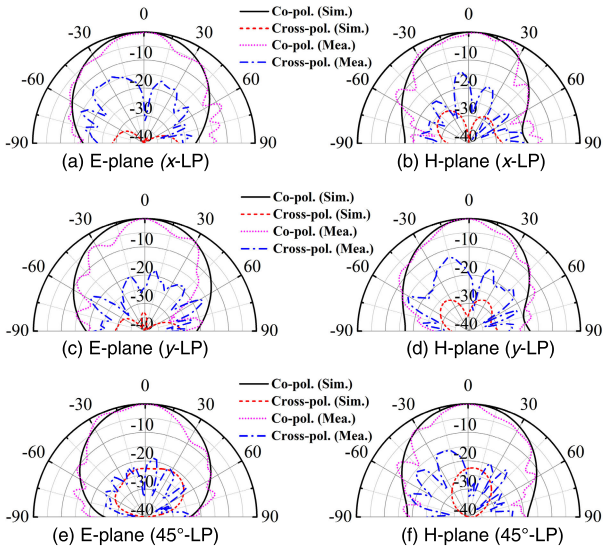

FIGURE 16. Simulated and measured E-plane and H-plane normalized radiation patterns of the proposed antenna at 5.2 GHz. (a) E-plane of *x*-LP. (b) H-plane of *x*-LP. (c) E-plane of *y*-LP. (d) H-plane of *y*-LP. (e) E-plane of 45°-LP. (f) H-plane of 45°-LP.

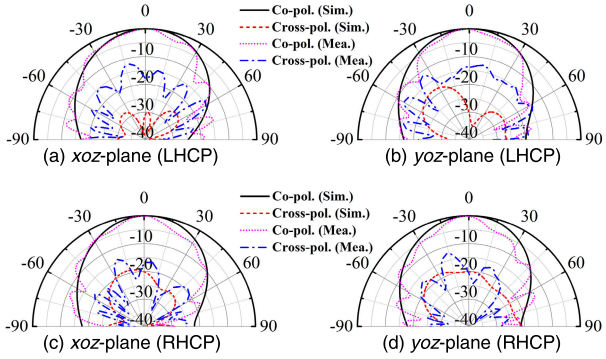

FIGURE 17. Simulated and measured *xoz*-plane and *yoz*-plane normalized radiation patterns of the proposed antenna at 5.2 GHz. (a) *xoz*-plane of LHCP. (b) *yoz*-plane of LHCP. (c) *xoz*-plane of RHCP. (d) *yoz*-plane of RHCP.

radiation patterns in two orthogonal principal planes at a lower frequency 4.8 GHz and the designed center frequency 5.2 GHz are plotted from Fig. 14 to Fig. 17. In general, the measured results have the broadside radiation patterns, which are in reasonable accordance with the simulated ones. The fluctuation of the measurement curves is caused by misalignment of the probe and environmental noise. Finally, the performance comparison between this work and previous works is listed in Table 4. Compared to previous antennas, the proposed antenna can obtain broadband, low profile and penta-polarization reconfigurability simultaneously.

IV. CONCLUSION

In this paper, a penta-polarization reconfigurable antenna based on mushroom-type metamaterial with crossed H-shape coupled slot is proposed. First, four radiation structures and the MTM with slot are analyzed by CMA, which gives the potential performance of the radiating structures. Based on the CMA, a broadband low-profile dual LP antenna is designed. Then a reconfigurable feeding network is designed. Through shifting the states of six SPST switches, the polarization of antenna can be switched among *x*-LP, *y*-LP, 45°-LP, LHCP and RHCP. Finally, the prototype with a profile of $0.06\lambda_0$ at 5.2 GHz is simulated and measured. The measured 10-dB impedance bandwidths are higher than 33.2% for LPs and higher than 38.7% for CPs. The measured axial ratio bandwidths are over 28%. With the MTM, the measured maximum boresight gains of all states are higher than 8.2 dBi. The advantage of the proposed antenna is to achieve a balance among low-profile, broadband and penta-polarization reconfigurability. In view of the advantages above, the proposed antenna has further applications in the fields of polarization diversity and C band satellite communication.

REFERENCES

[1] W. Lin and H. Wong, "Polarization reconfigurable wheel-shaped antenna with conical-beam radiation pattern," *IEEE Trans. Antennas Propag.*, vol. 63, no. 2, pp. 491–499, Feb. 2015.
[2] Y.-M. Cai, S. Gao, Y. Yin, W. Li, and Q. Luo, "Compact-size low-profile wideband circularly polarized omnidirectional patch antenna with reconfigurable polarizations," *IEEE Trans. Antennas Propag.*, vol. 64, no. 5, pp. 2016–2021, May 2016.
[3] Y. Shi, Y. Cai, X.-F. Zhang, and K. Kang, "A simple tri-polarization reconfigurable magneto-electric dipole antenna," *IEEE Antennas Wireless Propag. Lett.*, vol. 17, no. 2, pp. 291–294, Feb. 2018.
[4] H. L. Zhu, S. W. Cheung, X. H. Liu, and T. I. Yuk, "Design of polarization reconfigurable antenna using metasurface," *IEEE Trans. Antennas Propag.*, vol. 62, no. 6, pp. 2891–2898, Jun. 2014.
[5] C. Ni, M. S. Chen, Z. X. Zhang, and X. L. Wu, "Design of frequency- and polarization-reconfigurable antenna based on the polarization conversion metasurface," *IEEE Antennas Wireless Propag. Lett.*, vol. 17, no. 1, pp. 78–81, Jan. 2018.
[6] W. Li, S. Gao, Y. Cai, Q. Luo, M. Sobhy, G. Wei, J. Xu, J. Li, C. Wu, and Z. Cheng, "Polarization-reconfigurable circularly polarized planar antenna using switchable polarizer," *IEEE Trans. Antennas Propag.*, vol. 65, no. 9, pp. 4470–4477, Sep. 2017.
[7] S. W. Lee and Y. J. Sung, "Simple polarization-reconfigurable antenna with T-shaped feed," *IEEE Antennas Wireless Propag. Lett.*, vol. 15, pp. 114–117, 2016.
[8] H. H. Tran, N. Nguyen-Trong, T. T. Le, and H. C. Park, "Wideband and multipolarization reconfigurable crossed bowtie dipole antenna," *IEEE Trans. Antennas Propag.*, vol. 65, no. 12, pp. 6968–6975, Dec. 2017.
[9] J.-S. Row and Y.-H. Wei, "Wideband reconfigurable crossed-dipole antenna with quad-polarization diversity," *IEEE Trans. Antennas Propag.*, vol. 66, no. 4, pp. 2090–2094, Apr. 2018.
[10] H. H. Tran, N. Nguyen-Trong, T. T. Le, A. M. Abbosh, and H. C. Park, "Low-profile wideband high-gain reconfigurable antenna with quad-polarization diversity," *IEEE Trans. Antennas Propag.*, vol. 66, no. 7, pp. 3741–3746, Jul. 2018.
[11] W. Lin and H. Wong, "Polarization reconfigurable aperture-fed patch antenna and array," *IEEE Access*, vol. 4, pp. 1510–1517, 2016.
[12] W.-W. Yang, X.-Y. Dong, W.-J. Sun, and J.-X. Chen, "Polarization reconfigurable broadband dielectric resonator antenna with a lattice structure," *IEEE Access*, vol. 6, pp. 21212–21219, 2018.
[13] L.-Y. Ji, P.-Y. Qin, Y. J. Guo, C. Ding, G. Fu, and S.-X. Gong, "A wideband polarization reconfigurable antenna with partially reflective surface," *IEEE Trans. Antennas Propag.*, vol. 64, no. 10, pp. 4534–4538, Oct. 2016.
[14] R. Lian, Z. Tang, and Y. Yin, "Design of a broadband polarization-reconfigurable Fabry–Pérot resonator antenna," *IEEE Antennas Wireless Propag. Lett.*, vol. 17, no. 1, pp. 122–125, Jan. 2018.
[15] J. Hu, G. Q. Luo, and Z.-C. Hao, "A wideband quad-polarization reconfigurable metasurface antenna," *IEEE Access*, vol. 6, pp. 6130–6137, 2018.
[16] C. L. Holloway, E. F. Kuester, J. A. Gordon, J. O'hara, J. Booth, and D. R. Smith, "An overview of the theory and applications of metasurfaces: The two-dimensional equivalents of metamaterials," *IEEE Antennas Propag. Mag.*, vol. 54, no. 2, pp. 10–35, Apr. 2012.

[17] W. Liu, Z. N. Chen, and X. Qing, "Metamaterial-based low-profile broadband mushroom antenna," *IEEE Trans. Antennas Propag.*, vol. 62, no. 3, pp. 1165–1172, Mar. 2014.
[18] W. Liu, Z. N. Chen, and X. Qing, "Metamaterial-based low-profile broadband aperture-coupled grid-slotted patch antenna," *IEEE Trans. Antennas Propag.*, vol. 63, no. 7, pp. 3325–3329, Jul. 2015.
[19] W. E. I. Liu, Z. N. Chen, X. Qing, J. Shi, and F. H. Lin, "Miniaturized wideband metasurface antennas," *IEEE Trans. Antennas Propag.*, vol. 65, no. 12, pp. 7345–7349, Dec. 2017.
[20] Q. Chen, H. Zhang, Y.-J. Shao, and T. Zhong, "Bandwidth and gain improvement of an L-shaped slot antenna with metamaterial loading," *IEEE Antennas Wireless Propag. Lett.*, vol. 17, no. 8, pp. 1411–1415, Aug. 2018.
[21] F. H. Lin and Z. N. Chen, "Low-profile wideband metasurface antennas using characteristic mode analysis," *IEEE Trans. Antennas Propag.*, vol. 65, no. 4, pp. 1706–1713, Apr. 2017.
[22] M. Ameen and R. Chaudhary, "Metamaterial-based wideband circularly polarised antenna with rotated V-shaped metasurface for small satellite applications," *Electron. Lett.*, vol. 55, no. 7, pp. 365–366, Apr. 2019.
[23] M. Ameen, O. Ahmad, and R. Chaudhary, "Wideband circularly-polarised high-gain diversity antenna loaded with metasurface reflector for small satellite applications," *Electron. Lett.*, vol. 55, no. 15, pp. 829–831, Jul. 2019.
[24] Y. Chen and C. F. Wang, *Characteristic Modes: Theory and Applications in Antenna Engineering*. New York, NY, USA: Wiley, 2015.
[25] *M/A-COM Datasheet for MA4FCP300*. Accessed: Apr. 27, 2019. [Online]. Available: http://www.alldatasheet.com/datasheet-pdf/pdf/301848/MA-COM/MA4FCP300.html
[26] S. Sun, W. Jiang, S. Gong, and T. Hong, "Reconfigurable linear-to-linear polarization conversion metasurface based on PIN diodes," *IEEE Antennas Wireless Propag. Lett.*, vol. 17, no. 9, pp. 1722–1726, Sep. 2018.
[27] B. Yen Toh, R. Cahill, and V. Fusco, "Understanding and measuring circular polarization," *IEEE Trans. Edu.*, vol. 46, no. 3, pp. 313–318, Aug. 2003.

PENG LIU was born in Shanxi, China, in July 1993. He received the bachelor's degree in electromagnetic field and wireless technology from Xidian University, Xi'an, China, in 2016, where he is currently pursuing the Ph.D. degree. His current research interests include high-performance and multifunctional antenna based on metamaterial.

WEN JIANG (Member, IEEE) was born in Shandong, China, in November 1985. He received the bachelor's and Ph.D. degrees from Xidian University, Xi'an, China, in 2008 and 2012, respectively. He is currently the Vice Director with the National Key Laboratory of Science and Technology on Antennas and Microwaves, Xidian University, where he is also a Full Professor. His current research interests include electromagnetic scattering theory and technology, antenna theory and engineering, and electromagnetic measurement theory and technology.

SHANGYI SUN was born in Shaanxi, China, in July 1994. He received the bachelor's and master's degrees from the School of Electronic Engineering, Xidian University, Xi'an, China, in 2016 and 2019, respectively. His main research interests include metasurface and its applications in high performance or multifunctional antenna.

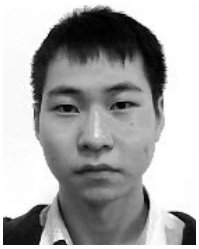

YAN XI was born in Shaanxi, China, in 1995. He received the bachelor's degree in industrial design from Xidian University, Xi'an, China, in 2017, where he is currently pursuing the Ph.D. degree in electromagnetic field and microwave technology with the School of Electronic Engineering. His current research interests include metasurface and their radiation and scattering applications.

SHUXI GONG (Member, IEEE) was born in Hebei, China, in March 1957. He received the bachelor's and master's degrees from Xidian University, Xi'an, China, in 1982 and 1984, respectively, and the Ph.D. degree from Xi'an Jiaotong University, Xi'an, in 1988. He was the Director with the National Key Laboratory of Science and Technology on Antennas and Microwaves, Xidian University, where he is currently a Full Professor. He has authored or coauthored more than 200 refereed journal articles. He has also authored *Principles of Generalized Eigenfunction Expansions in Electromagnetic Theory* (Xi'an: Xidian University Press, 2010), *Prediction and Reduction of Antenna Radar Cross Section* (Xi'an: Xidian University Press, 2010), and *Antennas for Mobile Communication Systems* (Beijing: Electronics Industry Press, 2011). His current research interests include antenna theory and technology, prediction and control of antenna radar cross section (RCS), and RCS calculation of complex targets.

Dr. Gong is a Senior Member of the Chinese Institute of Electronics (CIE) and a Vice Chairman of the Antenna Society of CIE. He was a recipient of the Science and Technology Advancement Award of Shaanxi Province, the Science and Technology Advancement Award of the Ministry of Information Industry of China, the Yilida Best Paper Award of Chinese Journal of Radio Science, the Outstanding Young Scholar Award of the Ministry of Mechanical Electronics of China, and the Excellent Young Backbone Teacher Award of the National Education Committee of China. He is an Editorial Board Member of the *Chinese Journal of Xidian University* and the *Journal of Microwaves*.